Eur Biophys J (2001) 30: 471–475
DOI 10.1007/s002490100169

BIOPHYSICS LETTER

Hermann Hartmann · André Bongers · Heinz Decker

Small-angle neutron scattering reveals an oxygen-dependent conformational change of the immunogen keyhole limpet hemocyanin type 1 (KLH1)

Received: 28 December 2000 / Revised version: 10 May 2001 / Accepted: 22 May 2001 / Published online: 21 July 2001

Abstract The respiratory protein of the keyhole limpet, *Megathura crenulata*, the hemocyanin (KLH), commonly used as an immunogen, binds oxygen cooperatively, which implies the existence of different conformations. For the first time, two different conformations of KLH1 were detected upon oxygenation, a deoxy and an oxy state, using small-angle neutron scattering. Rearrangements in the quaternary structure of KLH1 were predicted from the different radii of gyration and the shifts of the minima and maxima in the scattering curves. Upon oxygenation, KLH1 becomes smaller and more compact. Model reconstruction of KLH1 indicates a hollow cylinder with two rings located close to both ends, which move slightly together upon oxygenation.

Keywords Keyhole limpet hemocyanin · Small-angle neutron scattering · Immunogen · Oxygen-dependent conformations

Abbreviations *FU*: functional unit · *KLH*: keyhole limpet hemocyanin · *SANS*: small-angle neutron scattering

Introduction

The hemocyanin respiratory proteins are large, multisubunit copper proteins with molecular masses ranging between 0.5 and 8 MDa (Salvato and Beltramini 1990; Markl and Decker 1992; van Holde and Miller 1995; van Holde et al. 2001). They occur freely dissolved in the hemolymph of arthropods and molluscs to guarantee a precise oxygen delivery. Depending on the species, multimers of hexamers (1×6-mer, 2×6-mer, 4×6-mer, 6×6-mer, 8×6-mer) have been found in arthropods. In molluscs, decamers or didecamers or even larger multidecamers are found.

The hemocyanin of the keyhole limpet hemocyanin (KLH) from the marine gastropod *Megathura crenulata* is of particular interest since it is widely used as a hapten carrier and as a potent adjuvant immunostimulant. Because of these properties, KLH hemocyanin is also under clinical investigation as a therapeutic agent in the treatment of bladder carcinoma (Harris and Markl 1999, 2000; Jurincic-Winkler et al. 2000; Lamm et al. 2000). Two different hemocyanin isoforms, KLH1 and KLH2, have been found in the hemolymph with molecular masses of about 8 MDa, as determined by scanning transmission electron microscopy (Söhngen et al. 1997). Electron microscopy has revealed a similar quaternary structure for KLH1 and KLH2: a hollow cylinder with an outer diameter of about 360 Å and two inner rings near to both ends of the cylinder (Orlova et al. 1997). The smallest stable oligomer is a decamer with a height of 200 Å consisting of 10 elongated subunits. While KLH2 tends to assemble in didecamers and multidecamers, KLH1 forms predominantly didecamers (Gebauer et al. 1994). Each subunit has eight copper-containing functional units (FUs) of about 50 kDa and each FU binds one molecule of oxygen (van Holde and Miller 1995; Swerdlow et al. 1996). All eight FUs are different in their structure since they do not cross-react immunogelelectrophoretically (Markl 1994). This FU heterogeneity has also been observed for the hemocyanin subunit of the closely related cephalopode *Octopus dofleini*, of which all FUs have been sequenced (Miller et al. 1998). From the X-ray structure of *O. dofleini* FU-g, a FU of molluscan hemocyanin seems to contain two sub-domains with different folding motifs, an N-terminal α-helical part containing the oxygen binding center and a C-terminal β-rich part (Cuff et al. 1998; Miller et al. 1998).

While a lot of structural information is available about KLH, not much is known about the functional properties. In vivo, KLH1 and KLH2 serve as oxygen

H. Hartmann · A. Bongers · H. Decker (✉)
Institut für Molekulare Biophysik, Universität Mainz,
Jakob Welder Weg 26, 55128 Mainz, Germany
E-mail: decker@biophysik.biologie.uni-mainz.de
Tel.: +49-6131-3923570
Fax: +49-6131-3923557

carriers which are freely dissolved in the hemolymph. The existence of different conformational states of KLH was expected from the fact that the two KLH types bind dioxygen cooperatively (Senozan et al. 1981; Senozan and Briggs 1989; Swerdlow et al. 1996). However, no structural differences upon oxygenation have yet been detected.

A suitable method to detect conformational changes of large proteins in solution is small-angle solution scattering (SAS). It has successfully been applied to monitor changes of the quaternary structures of a number of allosteric proteins such as GroEL (Stegmann et al. 1998) and F_1-ATPase (Svergun et al. 1998). We have investigated KLH1 in solution in the absence and presence of molecular oxygen by small-angle neutron scattering (SANS), revealing changes in the quaternary structure.

Material and methods

Sample preparation

KLH1 was kindly provided by Dr. J. Markl, University of Mainz. It was purified according to Gebauer et al. (1994). Its didecameric oligomeric state was confirmed by transmission electron microscopy.

KLH1 in D_2O was obtained by dialysis against a buffer containing 99.7% (v/v) D_2O, 50 mM Tris, 5 mM $MgCl_2$, 5 mM $CaCl_2$ and 150 mM NaCl adjusted with HCl to pH 7.4. The deoxygenation of the KLH1 samples was performed with nitrogen gas in a glove box. Because of the high oxygen affinity of KLH1, the partial oxygen pressure had to be kept below 1 Torr to reach complete deoxygenation within 45 min. The deoxygenation was judged to be complete when the oxygen-dependent absorbance at 340 nm disappeared. During this procedure the protein concentration increased by evaporation of some D_2O. In order to work with the same concentration for the oxygenated sample, an aliquot of the deoxygenated protein solution was re-oxygenated in a small cap within minutes. The protein concentration was measured by light absorption at 278 nm. Using the extinction coefficient of 0.62 cm^{-1} mg^{-1} mL for KLH1, the protein concentration was determined to be 5.2 mg mL^{-1} and 5.0 mg mL^{-1} for the oxygenated and deoxygenated samples. No evidence for denaturation was detected during the deoxygenation process since no turbidity was observed and the spectra between 250 nm and 290 nm did not change.

Scattering experiments

The neutron scattering experiments were performed with the instrument D11 at the ILL in Grenoble, France. SANS data in the q range from 0.002 $Å^{-1}$ to 0.16 $Å^{-1}$ were measured at three distances, 18 m, 5 m and 2 m, with a wavelength $\lambda = 7.00$ Å and $\Delta\lambda/\lambda = 0.1$. The momentum transfer q is given by $4\pi\lambda^{-1}\sin(\theta/2)$, with θ denoting the scattering angle. The protein and control samples such as buffer were mounted on one sample holder and were measured several times to exclude possible changes of the conditions during the experiment. Data reduction and correction were done with standard ILL programs. Deconvolution of the radially averaged intensities with the resolution function (desmearing) was done by indirect Fourier transformation (Svergun et al. 1995). The integrity of the protein after the experiment was checked by comparing different time frames of the measured intensities and by transmission electron microscopy (TEM). In the D_2O samples a small fraction of higher oligomers was detected on the TEM pictures for both the oxygenated as well as the deoxygenated KLH1. The tubular aggregates gave a visible contribution to the SANS intensities below $q = 0.005$ $Å^{-1}$. These data points, measured only at the sample-detector distance of 18 m, were therefore excluded from all calculations.

Model building

Two different methods were used to simulate or to fit the small-angle data. For both methods described below the discrepancy:

$$\chi^2 = \frac{1}{N-n}\sum_{i=1}^{N}\left[\frac{sI_{\mathrm{mod}}(q_i) - I_{\exp}(q_i)}{\sigma(q_i)}\right]^2 \quad (1)$$

was minimized, where N is the number of data points, n the number of parameters and $I_{\exp}$ the desmeared experimental intensity with standard deviation σ. The intensity calculated from the protein model is given by I_{mod} and s denotes a scale factor.

Fit of a hollow cylinder

For a simple hollow cylinder the scattered intensity can be calculated analytically from three parameters: the length and the outer and inner radii of the cylinder. By a least-squares optimization of these parameters, the overall dimensions of KLH1 were determined, but due to the simplicity of the model the data could be fitted only in the lowest resolution shells (Fig. 1c).

Fit of a hollow cylinder with two additional cylindrical rings

Model building and calculation of the small-angle intensities were performed according to Henderson (1996). A hollow cylinder and two concentric rings within the cylinder (Fig. 2) were filled with randomly distributed scattering points. A mirror-plane symmetry was assumed for the model (Fig. 2). The small-angle intensity was calculated by a sine transform of the distance distribution function or directly with the Debye equation:

$$I(q) = \sum_i \sum_j f_i f_j \frac{\sin(qr_{ij})}{qr_{ij}} \quad (2)$$

where f denotes the scattering length assigned to a point, r_{ij} the distance between two points and q is given by $4\pi\lambda^{-1}\sin(\theta)$. The calculated intensities were fitted to the experimental data by a least-squares optimization (Eq. 1) of the six geometric parameters for the model: the lengths of the cylinder (L) and the ring (L_r), the outer (R_a) and inner (R_i) radius of the cylinder, the inner radius (R_{ir}) of the ring and the position of the ring (S) along the cylinder axis (see Fig. 2). The outer radius of the ring was fixed to the inner radius of the hollow cylinder. Because anisotropic scaling parameters such as height and radius were fitted, the distribution of scattering points was not considered to be isotropic after the parameters had changed by more than a few percent from the starting values. In this case a new starting model with the actual parameters, but with a random distribution of points, was generated for the next refinement cycles. The fraction of mass within the rings was determined by two approaches. In one approach the volume density of the scattering points was kept equal in the rings and the cylinder and the relative scattering length of the points in the ring was fitted. In the other approach the scattering lengths were kept identical and the density of points was varied.

Results and discussion

Figure 1a shows the small-angle scattering intensities of deoxygenated and oxygenated KLH1 as obtained by SANS. The differences between the scattering curves of

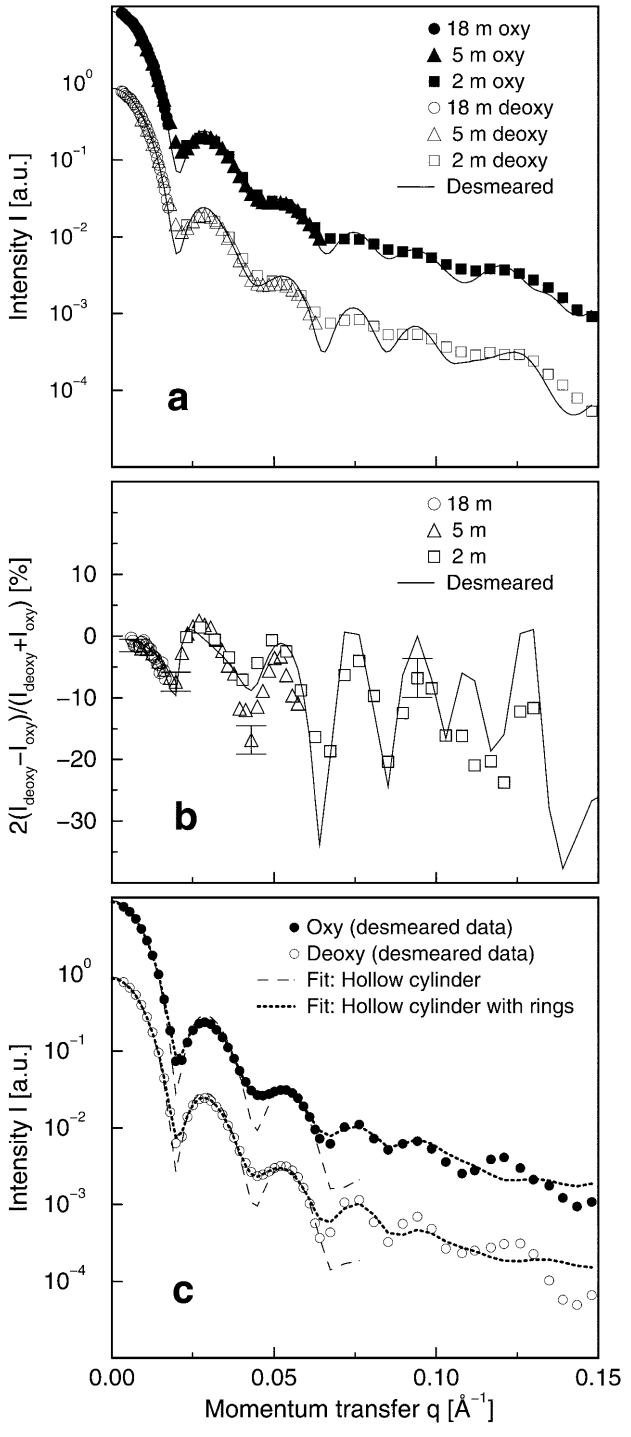

the oxy- and deoxy-KLH1 at different distances between the sample and the detector are shown in Fig. 1b. The oscillations of the differences are similar in independent experiments. In all cases the differences are well out of the range of experimental errors. It was not possible to explain the differences by changing the contributions of buffer and empty cuvette. Thus, the experimentally observed differences between oxy- and deoxy-KLH1 can therefore be regarded as highly significant.

◀

Fig. 1a–c SANS intensities of KLH1 in the presence and absence of oxygen. **a** The figure shows the raw intensities measured at three detector distances as well as the desmeared intensities of oxygenated and deoxgenated KLH1 in D_2O. For the sake of clarity, the intensities for deoxygenated KLH1 were divided by a factor of 10. **b** Relative differences between the scattered intensities of deoxygenated and oxygenated KLH1 measured at several sample-detector distances and the relative difference of the desmeared intensities. For the sake of clarity, the difference curve for the desmeared intensities was divided by a factor of two and the propagated experimental standard deviations are only shown for a few points. **c** Fitted scattering curves of the models for oxygenated KLH1 and deoxygenated KLH1 as given in Fig. 2 in comparison to the desmeared experimental intensities

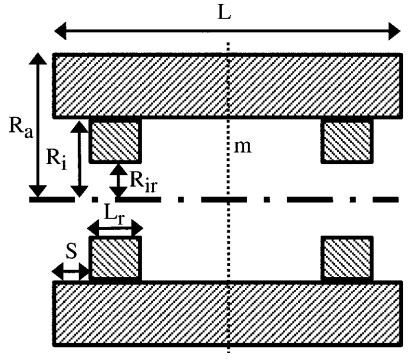

Fig. 2 Cross-section through a schematic model for the low-resolution shape of KLH1. The basic elements are a hollow cylinder and two cylindrical rings located within the cylinder. The fitted parameters (dimensions) of the model are shown in the figure. In this homogenous model the two decamers of KLH1 are connected by a mirror-plane symmetry

The minima and maxima in the scattering curves are less developed for the oxygenated form and they are shifted to higher q values by 1–2%. Since, in the case of cylindrically shaped molecules, deeper minima correspond to a more hollow cylinder while shallow minima indicate a more filled cylinder, one may state that masses are moved into the central hole of KLH1 molecules upon oxygenation.

The oxygen-dependent structural movements within the KLH1 molecule are also consistent with the observed changes in the radii of gyration. They were determined to 163.7 ± 0.5 Å for the oxy form and 165.0 ± 0.6 Å for the deoxy state, indicating that the oxy form of KLH1 is more compact than the deoxy form. These values are in good agreement with the radius of gyration ($R_g = 164$ Å) measured by small-angle X-ray scattering for a hemocyanin solution from the snail *Helix pomatia* (Pilz et al. 1974). Indirect Fourier transformation of the intensities gave distance distribution functions with a maximum size d_{max} for KLH1 of about 430 ± 10 Å for both the oxy and deoxy states.

Thus, although structural movements can be deduced within the quaternary structure of KLH1 upon oxygenation based on the differences in the R_g values and the difference plot, the molecular dimensions of KLH1 do not change within this error range.

Based on the absolute intensity of forward scattering, the molecular mass of KLH1 was determined to be 7.7 ± 0.7 MDa. This value is comparable to the mass of 8.3 MDa obtained by scanning transmission electron microscopy (Söhngen et al. 1997).

In order to model the shape of KLH1, in a first approach the small-angle scattering of a homogenous hollow cylinder was fitted to the SANS data. The fit resulted in high χ^2 values even in the low-resolution range ($\chi^2 = 78$ and $\chi^2 = 69$ for the oxy and deoxy data, respectively; $q < 0.075$ Å^{-1}) and there are large systematic deviations of the modeled intensities from the experimental curves (Fig. 1c). However, the dimensions obtained by this fit ($L = 360 \pm 10$ Å, $R_a = 161 \pm 3$ Å, $R_i = 85 \pm 5$ Å; compare Fig. 2) could be used as a first approximation for the point-scattering model (see above), which allowed the addition of two cylindrical rings (Fig. 2), representing the mass in the inner part of KLH1 as suggested by the reconstructed model from TEM (Orlova et al. 1997). The dimensions obtained are: $L = 375 \pm 3$ Å, $R_a = 155 \pm 1$ Å, $R_i = 100 \pm 1$ Å, $L_r = 46 \pm 2$ Å, $R_{ir} = 54 \pm 1$ Å, $S = 46 \pm 1$ Å for oxygenated KLH1 and $L = 370 \pm 2$ Å, $R_a = 156 \pm 1$ Å, $R_i = 98 \pm 1$ Å, $L_r = 44 \pm 2$ Å, $R_{ir} = 48 \pm 1$ Å, $S = 42 \pm 2$ Å for deoxygenated KLH1. Obviously, only minor changes in the quaternary structure of the KLH1 molecules occur upon oxygenation. The cylinder becomes slightly longer by about 5 Å and the rings are shifted in the direction of the molecular center by 4 Å or 10%. In addition, the thickness of the rings decreases from 50 Å to 46 Å. According to electron microscopy of molluscan hemocyanins, the 10 C-terminal located functional units g and h form the inner ring (Orlova et al. 1997; Meissner et al. 2000; Lieb et al. 2001). While larger rearrangements occur among these functional units, only minor movements can be observed within the 60 N-terminal located functional units building the wall of the cylinder. In contrast to the 4×6-meric arthropod hemocyanin from the spider *Eurypelma californicum*, the changes in the quaternary structure of this molluscan hemocyanin KLH1 are rather small (Decker et al. 1996).

For the fraction of mass in the rings we obtained 19% for both oxygenation states when the relative scattering lengths were fitted (see Materials and methods above) and 24% (21%) for oxygenated (deoxygenated) KLH1 when the density of scattering points was varied. In contrast to these results, the volume fraction of the rings is only about 11% in both models (oxygenated and deoxygenated KLH1). This discrepancy by a factor of two can be explained by assuming that the protein domains contributing to the rings are densely packed, whereas the (more or less spherical) domains forming the wall of the cylinder occupy only about 50% of the available volume by incorporating many holes in the wall as seen by electron microscopy (Orlova et al 1997; Meissner et al. 2000). There is a second argument for this assumption. With the dimensions of the models and using a density of 1.3 g cm^{-3} for KLH1, one would obtain a molecular mass of 15 MDa for KLH1. Assuming, however, that the packing density in the wall is only 0.5, a molecular mass of about 8 MDa was calculated for the models, in good agreement with the measured value (see above).

The comparison of the experimental SANS curves of deoxy-KLH1 and oxy-KLH1 revealed the existence of two structurally different conformations. Thus, a conformational change in the quaternary structure occurs in KLH1 upon oxygenation. Two possible oxygen-dependent conformations were also reported for another molluscan hemocyanin. In this case, however, optical diffraction was applied to TEM images of long tubular polymers, artificially produced from the didecameric hemocyanin of *Helix pomatia* (van Bremen et al. 1979).

Conclusion

For the first time, two different oxygen-dependent conformations have been revealed for a native molluscan hemocyanin in solution, the didecameric respiratory protein KLH1, a protein commonly used in immunology, medicine and biochemistry. The occurrence of at least two conformations is in accordance with the requirement of cooperative oxygen binding as reported for KLH1 (Swerdlow et al. 1996). From the desmeared intensities of the SANS experiments we obtained a decrease in the radius of gyration for the oxygenated state by 1.3 ± 0.7 Å. Therefore KLH1 seems to be slightly more compact in the oxygenated than in the deoxygenated state. Based on the difference of the radii of gyration, the differences in the scattering curves and the model reconstructions, structural changes between these two conformations can be deduced, which have not been observed by electron microscopy so far.

Acknowledgements We would like to thank Dr. R. May (ILL, Grenoble) and Dr. T. Nawroth (University of Mainz) for their help in performing the SANS experiments. We would also like to thank Dr. J.R. Harris (University of Mainz) and Dr. K. van Holde (Oregon State University), the latter for his help with the English language and very helpful criticism. This work was supported by Deutsche Forschungsgemeinschaft and the Centers for Science and Medical Research and of Material Science, Mainz.

References

Bremen JFL van, Ploegman JH, Bruggen EFJ van (1979) Structures of *Helix pomatia* oxy-hemocyanin and deoxy-hemocyanin tubular polymers. Eur J Biochem 100:61–65

Cuff ME, Miller KI, Holde K van, Hendrickson WA (1998) Crystal structure of a functional unit from octopus hemocyanin. J Mol Biol 278:855–870

Decker H, Hartmann H, Sterner R, Schwarz E, Pilz I (1996) Small-angle X-ray scattering reveals differences between the quaternary structures of oxygenated and deoxygenated tarantula hemocyanin. FEBS Lett 393:226–230

Gebauer W, Harris JR, Heid H, Süling M, Hillenbrand R, Söhngen S, Wegener-Strake A, Markl J (1994) Quaternary structure, subunits and domain pattern of two discrete forms of keyhole limpet hemocyanin: KLH1 and KLH2. Zoology 98:51–68

Harris JR, Markl J (1999) Keyhole limpet hemocyanin (KLH): a biomedical review. Micron 30:597–623

Harris JR, Markl J (2000) Keyhole limpet hemocyanin: molecular structure of a potent marine immunoactivator. A review. Eur Urol 37(Suppl S3):24–33

Henderson SJ (1996) Monte Carlo modeling of small-angle scattering data from non-interacting homogeneous and heterogeneous particles in solution. Biophys J 70:1618–1627

Holde K van, Miller MI (1995) Hemocyanins. Adv Protein Chem 47:1–81

Holde K van, Miller MI, Decker H (2001) Hemocyanins and invertebrate evolution. J Biol Chem 276:15563–15566

Jurincic-Winkler CD, Metz KA, Beuth J, Klippel KF (2000) Keyhole limpet hemocyanin for carcinoma in situ of the bladder: a long-term follow-up study. Eur Urol 37(Suppl S3):45–49

Lamm DL, Dehaven JI, Riggs DR (2000) Keyhole limpet hemocyanin immunotherapy of bladder cancer: laboratory and clinical studies. Eur Urol 37(Suppl S3):41–44

Lieb B, Altenhein B, Markl J, Vincent A, Olden E van, Holde K van, Miller KI (2001) Structures of two molluscan hemocyanin genes: significance for gene evolution. Proc Natl Acad Sci USA 98:4546–4551

Markl J (1994) Quaternary structure, subunits and domain patterns of two discrete forms of keyhole limpet hemocyanin: KLH1 and KLH2. Zoology 98:51–68

Markl J, Decker H (1992) Molecular structure of arthropodan hemocyanins. Adv Comp Environ Physiol 13:325–376

Meissner U, Dube P, Harris JR, Stark H, Markl J (2000) Structure of a molluscan hemocyanin didecamer (HtH1 from *Haliotis tuberculata*) at 12 Å resolution by cryoelectron microscopy. J Mol Biol 298:21–34

Miller KI, Cuff ME, Lang WF, Varga-Weisz P, Field KG, Holde K van (1998) Sequence of the octopus dofleini hemocyanin subunit: structural and evolutionary implications. J Mol Biol 278:827–841

Orlova EV, Dube P, Harris JR, Beckman E, Zemlin F, Markl J, Heel M van (1997) Structure of keyhole limpet hemocyanin type 1 (KLH1) at 15 Å resolution by electron cryomicroscopy and angular reconstitution. J Mol Biol 271:417–437

Pilz I, Engelborghs Y, Witters R, Lontie R (1974) Studies by X-ray small-angle scattering of the quaternary structure in solution of halves and tenths of *Helix pomatia* haemocyanin and of *Sepia officinalis* haemocyanin. Eur J Biochem 42:195–202

Salvato B, Beltramini M (1990) Hemocyanin molecular architecture: structure and reactivity of the binuclear copper-active site. Life Chem Rep 8:1–47

Senozan NM, Briggs M (1989) Hemocyanin levels in the giant keyhole limpet, *Megathura crenulata*, from the coast of California. Comp Biochem Physiol A 94:195–200

Senozan NM, Landrum J, Bonaventura J, Bonaventura C (1981) Hemocyanin of the giant keyhole limpet *Megathura crenulata*. In: Lamy J, Lamy J (eds) Invertebrate oxygen-binding proteins. Dekker, New York, pp 703–717

Söhngen SM, Stahlmann A, Harris JR, Müller S, Engel A, Markl J (1997) Mass determination, subunit organization and control of oligomerization states of keyhole limpet hemocyanin (KLH). Eur J Biochem 248:602–614

Stegmann R, Manakova E, Roessle M, Heumann H, Nieba-Axmann SE, Plückthun A, Hermann T, May RP, Wiedenmann A (1998) Structural changes of the *Escherichia coli* GroEL-GroES chaperonins upon complex formation in solution: a neutron small angle scattering study. J Struct Biol 121:30–40

Svergun DI, Semenyuk AV, Feigin LA (1995) Small-angle scattering data treatment by the regularization method. Acta Crystallogr Sect A 44:244–250

Svergun DI, Aldag I, Sieck T, Altendorf K, Koch MJ, Kane DJ, Kozin MB, Grüber G (1998) A model of the quaternary structure of the *Escherichia coli* F1 ATPase from X-ray solution scattering and evidence for structural changes in the delta subunit during ATP hydrolysis. Biophys J 75:2212–2219

Swerdlow R, Ebert RF, Lee PL, Bonaventura C, Miller KI (1996) Keyhole limpet hemocyanin: structural and functional characterization of two different subunits and multimers. Comp Biochem Physiol B 113:537–548